Ratiometric Near Infrared Fluorescence Imaging of Dopamine with 1D and 2D nanomaterials

Bjoern Hill[1§], Jennifer M. Mohr[1§], Isabelle K. Sandvoss[1†§], Juliana Gretz[1], Phillip Galonska[1], Lena Schnitzler[1‡], Luise Erpenbeck[2], Sebastian Kruss[1,3*]

[1] Department of Chemistry, Ruhr Universität Bochum, 44801Bochum, Germany
[2] Department of Dermatology, University Hospital Münster, 48149 Münster, Germany
[3] Fraunhofer Institute for Microelectronic Circuits and Systems, 47057 Duisburg, Germany

KEYWORDS: Biosensors, fluorescence, near infrared, ratiometric, nanosheets, carbon nanotubes, dopamine, neuroscience

ABSTRACT: Neurotransmitters are released by neuronal cells to exchange information. Resolving their spatiotemporal patterns is crucial to understand chemical neurotransmission. Here, we present a ratiometric sensor for the neurotransmitter dopamine that combines Egyptian Blue ($CaCuSi_4O_{10}$) nanosheets (EB-NS) and single-walled carbon nanotubes (SWCNTs). They both fluoresce in near infrared (NIR), which is beneficial due to ultra-low background and phototoxicity. $(GT)_{10}$-DNA functionalized monochiral (6,5)-SWCNTs increase their fluorescence (1000 nm) in response to dopamine, while EB-NS serves as stable reference (936 nm). A robust ratiometric imaging scheme is implemented by directing these signals on two different NIR sensitive cameras. Additionally, we demonstrate stability against mechanical perturbations and image dopamine release from differentiated dopaminergic Neuro 2a cells. Therefore, this technique enables robust ratiometric and non-invasive imaging of cellular responses.

Fluorescent materials are important in many applications for example as optical labels or molecular sensors. In particular, near-infrared (NIR) fluorescence offers several advantages for the study of biological systems[1,2]. In the NIR autofluorescence as well as absorption and scattering is greatly reduced compared to visible light[2]. Therefore, signals in the NIR show higher tissue penetration, better signal-to-noise ratios and substantially lower phototoxicity[1].

One NIR fluorescent material are single-walled carbon nanotubes (SWCNTs), which do not blink nor bleach[3]. Furthermore, SWCNTs can be chemically functionalised to detect a wide range of biomolecules[4]. SWCNTs can be conceptualized as rolled up graphene sheets of variable length[3–5]. Their (n,m)-chirality determines their optoelectronic properties and consequently in semiconducting SWCNTs their bandgap[3]. For example, (6,5)-SWCNTs possess an emission maximum close to 1000 nm but the exact emission wavelength depends on surface functionalization and solvent[4].

The NIR fluorescence of semiconducting SWCNTs is best described by excitons and very sensitive to the chemical environment[4,6]. This offers the possibility of using SWCNTs as building blocks for (bio)chemical sensors. In addition, to increase the colloidal stability of SWCNTs in polar solvents such as water non-covalent functionalization with DNA, peptides, proteins, or polymers has been employed[7–13].

Furthermore, functionalization tailors SWCNTs for analyte detection[4]. So far reactive oxygen species[14–18], small molecules[19–22], sugars[23], peptides[24], proteins[25–27], dopamine[28,29] and serotonin[30,31] and even pathogens[32,33] have been detected. SWCNTs offer high spatiotemporal resolution, making them suitable for imaging as well as cytometric approaches[34]. In addition to direct sensing, indirect sensing is performed, e.g. by detecting the product of an analyte's chemical reaction[14,35]. Ratiometric sensing with SWCNTs provides an even more robust approach[6,33,36–40]. Beyond intensity-based sensing, there are emerging methods such as NIR fluorescence lifetime imaging (FLIM) using SWCNTs[41]. In addition to fluorescence as readout, SWCNTs can also be used as sensors for electrical signal transduction[42]. For long-term studies, SWCNTs can also be injected intravenously in mice and demonstrate high biocompatibility[43].

Commercially available SWCNTs contain mixtures of different chiralities and thus show spectral overlap and congestion. However, purified single chirality SWCNTs provide well-defined spectra. Thus, they promise sensing with even higher selectivity and sensitivity which makes them preferable[6,32,36]. Single chirality (6,5)-SWCNTs for example have already been used in various sensing applications showing benefits for biosensing [6,32,36–38].

Another promising NIR emitting fluorophore for biophotonics is based on Egyptian Blue ($CaCuSi_4O_{10}$, EB)[44,45]. EB is the oldest artificial pigment manufactured by mankind, it has been identified in artworks dating back to 2500 BC in ancient Egypt, where it was used to decorate various pieces of art[46,47]. At present times, EB is attracting interest as a novel NIR fluorophore. EB has a tetragonal crystal structure consisting of parallel layers of silicate tetrahedra weakly bound by calcium ions[48]. The photophysical properties of EB are attributed to copper ions (Cu^{2+}) being part of the silicate framework. Their $^2B_{2g}$-$^2B_{1g}$ electronic transition is causing the NIR fluorescence of EB[49]. Bulk EB has a broad excitation spectrum in the visible wavelength range, from 550-700 nm and emits fluorescence with remarkable stability at about 936 nm[45,49,50]. Furthermore, EB fluorescence is characterized by a very high quantum yield (up to 30 %) compared to typical NIR fluorescent dyes and a fluorescence lifetime (100–150 µs) longer than the vast majority of NIR fluorescent material[51–53]. Due to the weak interlayer bonds, it is possible to exfoliate EB into Egyptian Blue

nanosheets (EB-NS) for example by simple long-term stirring in hot water[44]. This approach has been improved by planetary ball milling and surfactant assisted bath sonication, which improved monodispersity[54]. Importantly, the characteristic NIR fluorescence remained constant upon exfoliation to EB-NS[55].

EB-NS offer great potential in the biomedical field for bioimaging, sensing, tissue engineering, or even photothermal therapy. The biocompatibility of EB-NS has been demonstrated by cell viability assays and *in vivo* studies[52,55]. Beyond, functionalization of EB-NS has been demonstrated and used for targeting of cells[56]. Due to its high brightness, the NIR fluorescence of EB-NS can be imaged even using standard Si-based cameras, which are less sensitive for NIR signals[52]. The remarkable stability of the EB-NS fluorescence provides further opportunities as reference material in ratiometric sensors[33].

One of the disadvantages of fluorescence measurements are perturbations by mechanical movements or variations in the light path or intensity. Ratiometric approaches using two (related) signals can improve accuracy and compensate for such external factors[57]. Ratiometric measurements mitigate such effects of environmental variations[58]. This self-referencing/self-calibrating property makes ratiometric sensors particularly robust and reliable in dynamic environments[59,60].

A variety of ratiometric probes/sensors based on organic fluorescent molecules have been developed for applications such as sensing, imaging and biomedical applications[58,61,62]. There are also a few examples of SWCNTs that have been used for ratiometric concepts especially using chirality enriched SWCNTs[6,32,36–38,40]. Here, one chirality serves as non-responsive reference and the other as analyte responding component. The sensor´s response to analytes as e.g. dopamine can be further tuned through SWCNT functionalization[29]. Thereby, the detection of nitric oxide, hydrogen peroxide, pyrophosphate, different pathogens, riboflavin, and dopamine has been shown[6,63]. Overall, ratiometric fluorescent sensors promise many advantages but their implementation for novel analytes as well as spectral unambiguity and robustness remains a challenge.

In this paper, we present a ratiometric sensing approach by combining the fluorescence properties of SWCNTS and EB-NS for the NIR imaging of catecholamines such as dopamine.

Experimental

Exfoliation of EB to EB-NS

The exfoliation process from EB powder to EB-NS was carried out as previously shown in a two-step exfoliation procedure[54]. In the first step, 8 g of EB powder (Kremer Pigmente) was introduced into a 50 mL agate grinding jar (Retsch) together with 200 5 mm agate grinding balls and 4 ml deionized water. The mixture was milled 4 times in a PM 100 planetary ball mill (Retsch) at 600 rpm for 15 min with 5 min cooling breaks in between. The resulting slurry was transferred to a reaction vessel and diluted with deionized water to a volume of 100 ml. To remove larger particles, liquid phase centrifugation was applied. The necessary centrifugation parameters were calculated with a modified Stokes equation[52].

$$t = \frac{18 * \eta}{(\rho_k - \rho_w) * 4\pi^2 * f^2 * d^2} \ln\left(\frac{r}{r_0}\right) \quad (1)$$

The variables are the settling time (t), the dynamic viscosity of medium (water, η), the grain density (ρ_k), the medium density (ρ_w), the rotation frequency (f), the grain diameter (d), the distance between the rotor's fulcrum and sediment's height (r) and the distance between the rotor's fulcrum and suspension's surface (r_0). To remove particles with a hydrodynamic radius (r_{hyd}) larger than 1 µm, 50 ml of the milled EB dispersion was centrifuged in a 50 ml reaction vessel (Sarstedt) using a 5810R Centrifuge (Eppendorf) equipped with an A-4-62 rotor (Eppendorf) for 4 min at 1650 rpm. After the centrifugation, the supernatant containing only nanoparticles $r_{hyd} \leq 1\mu m$ was decanted and stored whereas the pellet was resuspended in water. This centrifugation step was repeated five times while always storing the supernatant and redispersing pellet in each iteration.

For the second step the EB-NBS dispersion was diluted to a concentration of 2 mg/ml and sodium dodecyl benzyl sulfonate (SDBS, Sigma-Aldrich GmbH) was added at a concentration of 1 wt %. The so-obtained dispersion was sonicated in the ultrasonic bath Sonorex RK 103 (Bandelin Electronic). 15 ml of this dispersion was filled in a 25 ml glass bottle (Schott), which was then sealed with PTFE tape. Subsequently, the glass bottle was bath sonicated for 6 h at 60 °C. Afterwards, to achieve the desired size of EB-NS, more size selective centrifugation (30 ml dispersion in a 50 ml reaction vessel, 4 min at 2900 rpm) was conducted. The EB-NS were then dried and dispersed in ultrapure water in a subsequent short sonication step.

Preparation of SWCNTs samples

To obtain purified (6,5)-SWCNTs the SWCNTs were purified according to the aqueous two-phase extraction protocol by Li et al[64,65]. SWCNT chirality was separated in a three-step approach with the SWCNTs being in between two aqueous phases. The phases contained dextran (MW 70 kDa, 4 % m/m) and polyethylene glycol (MW 60 kDa, 8 % m/m) and varied in their pH values due to the addition of HCl. The final bottom phase yielded almost monochiral (6,5)-SWCNTs and was diluted with 1 % sodium deoxycholate (DOC) solution to ensure stability. To remove residual dextran polymer from the separation, the DOC-SWCNTs were dialyzed with a 300 kDa dialysis bag against 1 % DOC 5 times with a change of the 1 % DOC solution.

We then performed a surfactant exchange from DOC to $(GT)_{10}$ ssDNA, by combining 200 µl SWCNTs with 10 µl PEG 6k in 40 % water and 20 µl 2 mg/ml $(GT)_{10}$. Under vortexing, 200 µl MeOH was added dropwise to the mixture following by the addition of 530 µl isopropyl alcohol. The dispersion was then centrifuged for 2 min at 23000 g to remove the supernatant. The pellet was resuspended in PBS and sonicated in a bath sonicator until all components had dissolved. The centrifugation and resuspending cycles were repeated until the pellet no longer had a white sheen. The

pellet was allowed to dry. 50 µl PBS and 50 µl $(GT)_{10}$ (2 mg/ml in PBS) were added to the pellet and sonicated briefly to combine the components. This was followed by a tip sonication at 30 % amplitude for 20 min and a final centrifugation for 20 min at 23000 g. The final supernatant was collected and the SWCNT concentration was measured using a Jasco V-770 UV–visible/NIR spectrophotometer for absorbance measurements. Therefore, 0.5 % SDBS/SWCNTs solution was transferred to a 10 mm path polystyrene cuvette (SARSTEDT, Germany) and the absorbance was measured with a wavelength range of 400 nm to 1350 nm. From the E11 absorption feature the concentration was calculated by estimating the area under the curve using a method published elsewhere[66].

Preparation of the ratiometric NIR sensor

For the ratiometric sensor in dispersion 0.1 nM SWCNTs of CoMoCAT- or purified $(GT)_{10}$-(6,5)-SWCNTs were mixed with 0.76 mg/ml EB-NS in PBS and measured in a 96-glass bottom well plate (Thermo Fisher Scientific). For the ratiometric sensing on surface, 0.05 mg/ml EB-NS and 0.5 nM $(GT)_{10}$-(6,5)-SWCNTs were used. The nanomaterials were incubated for 30 min and afterwards, the glass was washed three times with PBS prior to measurement.

NIR Fluorescence spectroscopy

For NIR fluorescence spectroscopy a custom-made setup was used, containing a Gem 561 laser (Laser Quantum). The laser was focused into a IX73 microscope (Olympus) equipped with a 20x objective. For spectroscopy, a Shamrock 193i spectrograph (Andor Technology) coupled to an array NIR detector (Andor iDUs InGaAs 491) was connected to the microscope. For spectroscopy measurements, 200 µl of the respective sensor dispersions were placed in a 96-well plate with glass bottom and positioned above the objective. Fluorescence data was acquired via the Andor SOLIS software. The laser power was set to 100 mW, exposure time to 1 s and input slit width to 500 nm. Data analysis and plotting were performed using Python.

Ratiometric NIR Fluorescence imaging

For NIR fluorescence spectroscopy a custom-made setup was used, containing a Gem 561 laser (Laser Quantum). The laser was connected to a IX73 microscope (Olympus) equipped with a UPlanSApo 60x Oil Microscope Objective (Olympus). The fluorescence signal was split using a dichroic mirror with a cut-on wavelength of 955 nm (T 955 LPXR, AHF analysentechnik AG). The fluorescence then was captured using two cameras, for the signal λ<955 nm (EB-NS-channel) the PCO edge 4.2 bi (Excelitas) for the signal λ>955 nm (SWCNT-channel) the NIR InGaAs Camera XEVA (Xenics) was used.

Ratiometric NIR Fluorescence Analysis

To calculate the ratiometric image response, the images recorded by the two cameras for the measurements were analyzed using ImageJ. For this purpose, the videos were opened as a stack in ImageJ and the SWCNT-channel was divided by the EB-NS-channel. The first 10 (characterization on the surface) or 50 (with cells) images were averaged and subtracted from the rest of the image to obtain background-corrected images. This was then divided by the averaged image to obtain the ratiometric response. The ratiometric response was then colour-coded.

Cell Culture

Mouse Albino neuroblastoma (Neuro 2a) cells were cultured in Dulbecco's Modified Eagle Medium (DMEM, Gibco) supplemented with 10 % fetal bovine serum (FBS, Gibco), 1 % Penicillin/Streptomycin (Pen/Strep, Gibco) and 1 x MEM Non-Essential Amino Acids (neAA, Gibco), in a 37 °C incubator with 5 % CO_2. For differentiation 50000 cells were seeded in 35 mm glass dishes (Mattek) in RPMI 1640 medium without phenolred (Gibco) supplemented with 10 % FBS, 1 x neAA and 100 µM dibutyryl cyclic adenosine monophosphate (dbcAMP, Sigma) in a 37 °C incubator with 5 % CO_2 for 4 days.

Ratiometric NIR Fluorescence imaging of cells

The sensor was applied to the cells using a painting approach[67]. Prior to measuring the differentiation medium was removed and replaced with 1 nM purified (6,5)-SWCNTs and 0,05 mg/ml EB-NS in Hanks' Balanced Salt Solution (HBSS, Gibco) supplemented with 2 mM $CaCl_2$ and incubated for 10 min. The cells were carefully washed three times with HBSS with 2 mM $CaCl_2$ and placed on the microscope for imaging. The focus was adjusted to the optimal level for both SWCNTs and EB-NS. The same setup as mentioned above was used.

The cells were measured for 1 minute before 100 mM KCl was added to the calcium-enriched medium to ensure a background measurement. After the addition of KCl, the cells were imaged for additional 6 minutes. Ratiometric NIR fluorescence analysis was performed as described above.

Results and Discussion

Ratiometric sensor design

The exceptional stability of EB-NS fluorescence in the NIR suggests potential as reference material in ratiometric sensors as shown before with bulk EB[33]**.** The straightforward exfoliation of EB-NS as well as the low cost of EB is another advantage of this nanomaterial. In contrast, SWCNTs are very sensitive to their environment and the purification of single chirality SWCNTs is more challenging[6].

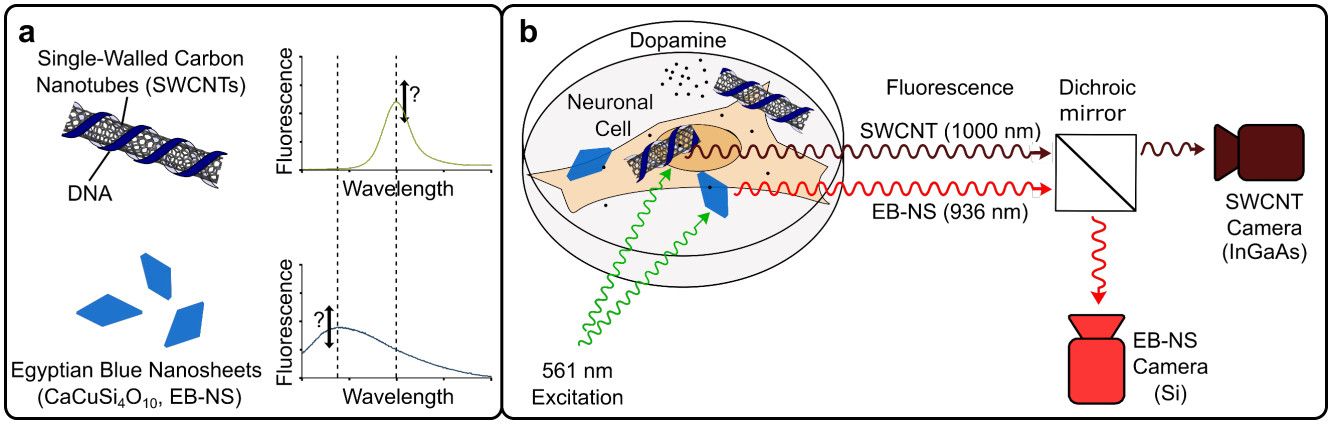

FIGURE 1: Schematic ratiometric sensor design and imaging concept: a) Interaction of the utilized nanomaterials with exposure to dopamine. Functionalized SWCNTs will show an increase of their fluorescence under exposure, the fluorescence of EB-NS remains unchanged. b) Ratiometric imaging setup: Both components of the nanosensor are adsorbed (painted) on the biological samples of interest. Upon excitation with visible green light (561 nm) they exhibit near-infrared fluorescence. The fluorescence signals of the two nanomaterials are separated by a dichroic mirror and the spatially and temporally resolved signals are imaged simultaneously on two different cameras.

Therefore, we decided to use EB-NS as a reference material and specifically functionalized SWCNTs as sensor material (Figure 1a). The goal of this sensor design was to use both materials for ratiometric imaging of the neurotransmitter dopamine in cell experiments (Figure 1b). In a simulation, we observed, that EB-NS and SWCNTs in a combination were suitable to use them as ratiometric sensors (Figure S1). For this purpose, we created an optical setup that allows parallel imaging of both fluorescence signals at the same time (Figure 1b). To produce a ratiometric sensor for dopamine we first established one material as non-reactive and one reactive component to the substance of interest (dopamine). For this purpose, SWCNTs were functionalized with single-stranded $(GT)_{10}$ DNA to make them sensitive to catecholamine neurotransmitters including dopamine[6,67]. Commercially available CoMoCAT-SWCNTs were measured before and after addition of dopamine. A fluorescence intensity increase of 110 % was observed at the peak wavelength at 999.5 nm (FIGURE 2a). In addition, fluorescence spectra of purified (6,5) SWCNTs, which were also functionalized with the same DNA sequences, were collected (FIGURE 2b). Here, fluorescence intensity increased by 260 % in response to dopamine EB-NS fluorescence spectra showed as expected no response to dopamine (FIGURE 2**Error! Reference source not found.**c).

To obtain a ratiometric sensor optimized for fluorescence spectroscopy measurements, both components were combined in such a way that the spectral maxima of 936.5 nm (EB-NS) and 999.5 nm (SWCNTs) were similar in height. We found concentrations of 0.76 mg/ml EB-NS and 0.1 nM SWCNTs to be optimal.

With commercially available CoMoCAT-SWCNTs the ratiometric sensor responded to dopamine (Figure 2d). However, the fluorescence increased only by 37 % and the broader spectrum of CoMoCAT-SWCNTs overlapped with the EB-NS signal, which makes signal changes ambiguous. In contrast, for the ratiometric sensor based on single chirality (6,5)-SWCNTs, the fluorescence increased by 280 %. Additionally, the spectral overlap is minimal because other chiralities other than (6,5), namely (8,3) and (7,6) did not congest the spectrum. The cleaner spectrum of monochiral SWCNTs was also visible in the absorption spectrum (Figure S2). In control measurements of the ratiometric sensors (Figure S3), we could not detect any changes in fluorescence in response to the buffer PBS. Usually, a normalized Intensity I_{norm} is calculated by subtracting the start intensity I_0 from the measured Intensity I:

$$I_{norm} = \frac{I - I_0}{I_0} \tag{1}$$

Here, the start intensity was calculated by averaging over the first values before analyte addition in order to compensate for any fluctuations. For our ratiometric approach I is substituted by the intensity ratio

$$R = \frac{I_{SWCNTs}}{I_{EBs}} \tag{2}$$

and with that the ratiometric response $R_{norm.rat.}$ can be defined as:

$$R_{norm.rat.} = \frac{R - R_0}{R_0} \tag{4}$$

With the intensity of the SWCNTs (I_{SWCNT}) and the Intensity of the EB-NS (I_{EB}) this equals:

$$R_{norm.rat.} = \frac{\frac{I_{SWCNT}}{I_{EB}} - \frac{I_{SWCNT,0}}{I_{EB,0}}}{\frac{I_{SWCNT,0}}{I_{EB,0}}} \tag{5}$$

For ratiometric sensing utilizing the fluorescence spectral intensities, a ratiometric spectral response was calculated based on the fluorescence intensities at 936.6 nm and 999.5 nm as I_{SWCNT} and I_{EB} respectively. When the

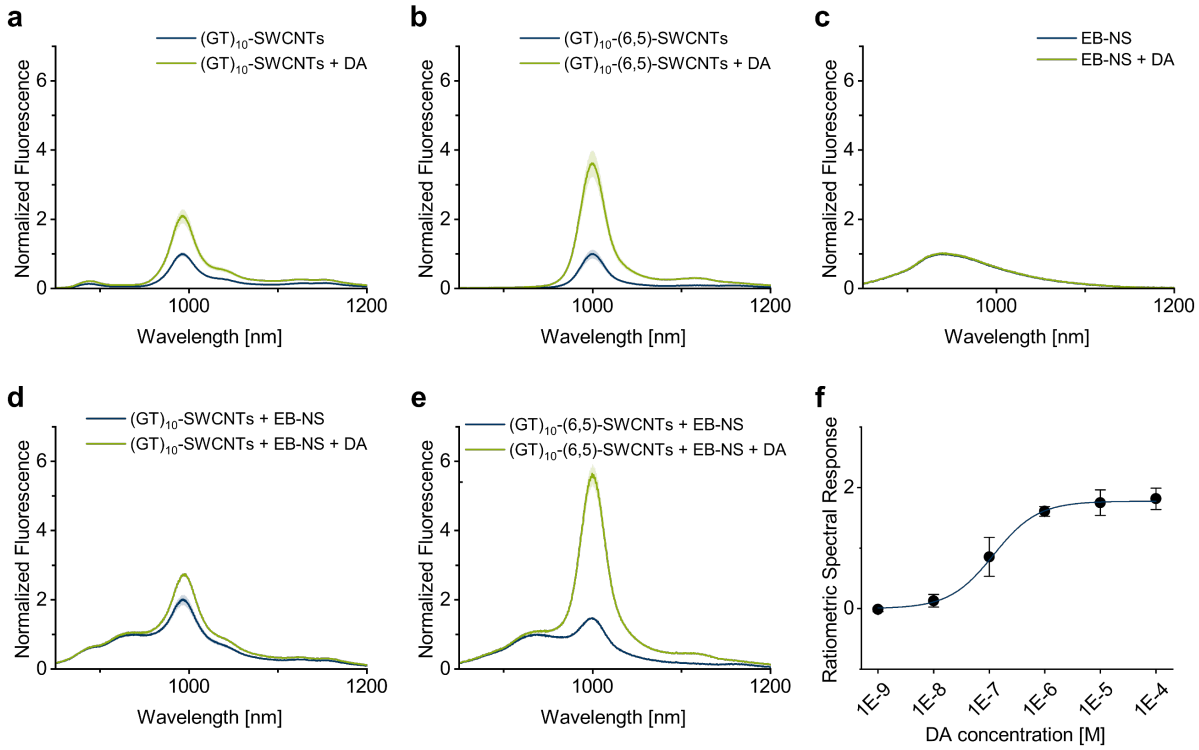

FIGURE 2: Ratiometric NIR sensing of dopamine in solution. a)-e): NIR-fluorescence spectra before and after the addition of (100 µM) dopamine (DA). Errors shown as shades = SD (n=3). a) NIR-fluorescence spectra of $(GT)_{10}$-SWCNTs (0.1 nM). b) NIR-fluorescence spectra of $(GT)_{10}$-(6,5)-SWCNTs (0.1 nM). c) NIR-fluorescence spectra of EB-NS (0.76 mg/ml). d) NIR-fluorescence spectra of a ratiometric sensor (EB-NS and $(GT)_{10}$-SWCNTs). e) NIR-fluorescence spectra of a ratiometric sensor (EB-NS and $(GT)_{10}$-(6,5)-SWCNTs). f) Calibration curve of a ratiometric sensor EB-NS and $(GT)_{10}$-(6,5)-SWCNTs), as ratiometric spectral response. The blue curve shows a sigmoidal fit given by Hill equation (R^2=0.994). Error bars = SD (n=3)

ratiometric sensor was read out using fluorescence microscopy, a ratiometric imaging response was calculated based on the intensity values of the two cameras employed as I_{SWCNT} and I_{EB} respectively. With the ratiometric spectrometric response the sensitivity of our sensor was determined (Figure 2f, Figure S4, Table S1) and it detected dopamine in the range from 10^{-9} M to 10^{-4} M.

Ratiometric sensing on surfaces

For cell experiments sensors are typically immobilized on the same surface as the cells or on the cells as so-called "paint". Therefore, we next characterized the ratiometric sensor on surfaces. For this purpose, the sensor was incubated on a glass surface and the performance was first measured by fluorescence spectroscopy and then via imaging. The microscopy setup included two cameras for simultaneous imaging. Because EB-NS fluorescence is closer to the visible we used a Si-based camera for EB-NS, while the fluorescence of the SWCNTs was captured by an InGaAs camera. To account for the broader spectral range of the EB-NS compared to the SWCNTs, and for the different detection levels of the two different cameras employed, the concentrations of EB-NS and SWCNTs were adjusted. The composition of the sensor was changed in a way that similar signal levels could be detected by both cameras. The EB-NS concentration was therefore lowered and the SWCNT concentration was increased due to the broader spectrum and higher quantum yield of the material and the camera. Finally, 0.05 mg/ml EB-NS and 0,5 nM purified (6,5)-$(GT)_{10}$-SWCNTs were incubated on a glass surface for 30 min and washed twice prior to measurements in PBS. The surface-coated ratiometric sensor showed a similar spectral response to dopamine as in solution (Figure 3a) and no response to PBS buffer (Figure S5).

In comparison to measurements in solution the spectral peaks were less intense as well as the change by dopamine, which can be attributed to the impact of the sensor density and glass substrate for example by local charges

Next, sensor responses were measured using fluorescence microscopy (Figure 3b, Figure S6, Table S2) and showed a sensitivity in the range of 10^{-8} M to 10^{-5} M. The lower response at high dopamine concentrations can be attributed to dopamine polymerization as reported before[68]. This ratiometric sensing enables spatially resolved imaging of the dopamine concentration (Figure 3c, Movie S1), as the ratiometric image response can be calculated for each pixel individually. As expected, signals of EB-NS in the Si-based camera did not alter upon dopamine addition. In contrast, SWCNTs became brighter.

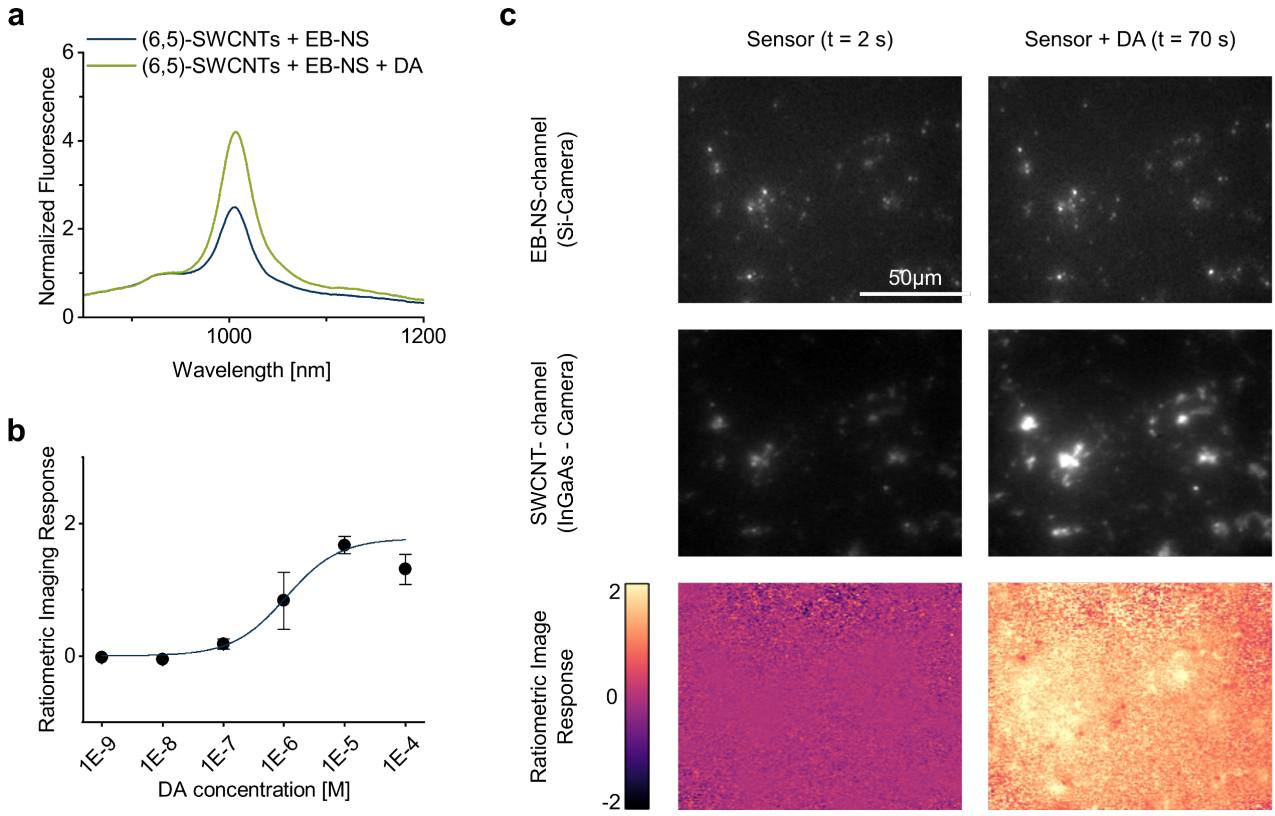

FIGURE 3: Ratiometric NIR sensing of dopamine on surfaces. a) NIR-fluorescence spectra of the adsorbed components of the ratiometric sensor before and after the addition of dopamine (100 µM) in PBS. b) Calibration curve of the adsorbed ratiometric sensor, as ratiometric image response. The blue curve shows a sigmoidal fit given by Hill equation (R^2=0.999). Error bars = SD (n=3). c) Fluorescence microscopy images of the adsorbed ratiometric sensor before and after the addition of dopamine (100 µM) in the two different channels and shown as ratiometric image response.

Benefits of ratiometric sensing and imaging

Next, we assessed the advantages of using a ratiometric approach. To quantify the robustness of the sensor to variations in light intensity without dopamine addition (**Error! Reference source not found.**a, Figure S7) images were recorded at different excitation power. For this, the excitation laser was tuned up to 22 mW. Both signals increased but the ratiometric response remained constant, which demonstrates one of the advantages of a ratiometric approach. Next, we tested the ratiometric response with a fluctuating excitation laser and the addition of dopamine over a time period of 80 s FIGURE 4b, c, Movie S2). The fluctuations can be used to simulate disturbances in the environment, such as an inhomogeneously absorbing medium. Again, the ratiometric response, was not influenced by laser fluctuations. Consequently, dopamine can be robustly detected by our approach.

Ratiometric imaging of dopamine release from neuronal cells

In a final step, the performance of the sensor was tested in a biological system with Neuro 2a cells. Neuro 2a cells originate from a neuroblastoma of the mouse neural crest and are used to study neuronal development, differentiation, etc.[69]. Various agents have been used to induce neuronal differentiation in Neuro 2a cells such as transforming growth factor beta1 (TGF beta 1), bone morphogenetic protein 4 (BMP4), glial cell-derived neurotrophic factor (GDNF) or retinoic acid (RA)[69]. Furthermore, dibutyryl cyclic adenosine monophosphate (dbcAMP) differentiates these cells into a dopaminergic phenotype[70].

Therefore, to study dopamine release we differentiated Neuro 2a cells into dopaminergic cells by applying dibutyryl cyclic adenosine monophosphate for four days and then incubated them with the ratiometric sensor for 10 min prior to measurement. First, the cells were imaged without a trigger and then dopamine release was triggered by adding KCl (100 mM), which caused Ca^{2+} influx into the cells and exocytosis[71]. For a precise localization of the cells, we took brightfield images (FIGURE 5a) and measured the fluorescence intensities of the selected areas (FIGURE 5b,c, Movie S3). In the EB-NS-channel there was no change in intensity over time, while in the SWCNT-channel intensity increased after stimulation around and under each cell. The ratiometric response showed that the cells release dopamine during stimulation, and we were able to monitor the release and extracellular diffusion of dopamine from each cell over time. Additionally, the ratiometric response of surfaces /sensors without cells, slightly decreased by the addition of KCl (Figure S8), but there was a strong increase of the ratiometric image response with cells (FIGURE 5d). This indicates an intensity change triggered by the dopamine exocytosis of the cells by KCl, although the trigger substance slightly quenches the SWCNT's fluorescence.

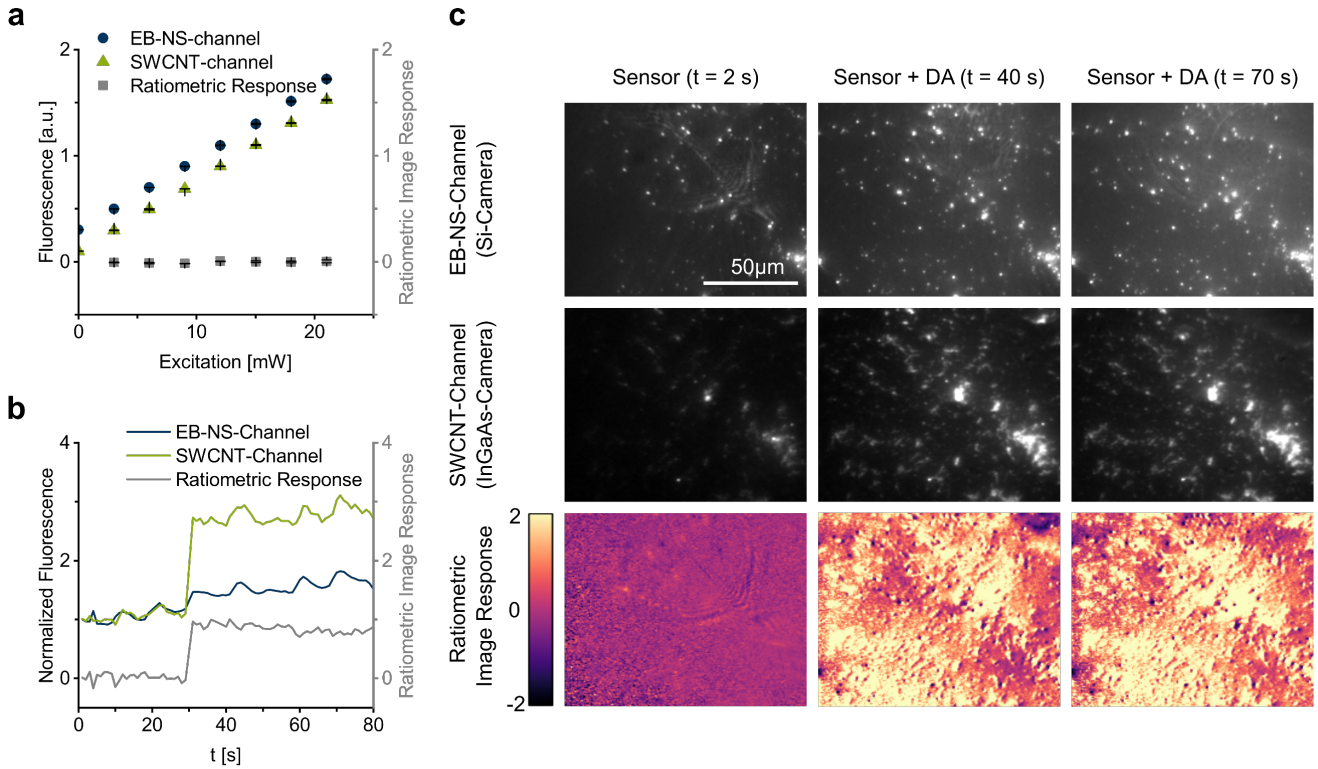

FIGURE 4: Robustness of the ratiometric sensor to perturbations. a) Image intensities for varying excitation power. Error bars = SD (n=3). b) Image intensities for varying excitation power and upon addition of dopamine (100 µM). c) Corresponding fluorescence microscopy images at different time points for varying excitation power and upon addition of dopamine (100 µM).

The integration of EB-NS and SWCNTs into a ratiometric sensor ensures increased sensitivity and selectivity for the detection of dopamine even in complex cellular environments. The synergistic interaction of nanosheets and nanotubes minimizes interference from cellular components and provides a clear and specific signal triggered by dopamine release from the differentiated Neuro 2a cells upon KCl stimulation[72]. This enables the monitoring of exocytosis events in real time, e.g. the release of dopamine triggered by a stimulus. In addition, good temporal (up to 10 frames per second) and spatial resolution can be achieved as already seen with other SWCNT biosensors[4,67,73,74]. Furthermore, ratiometric sensors can also be used in different cell types[75].

A NIR fluorescent sensor provides several advantages compared to other methods such as HPLC, genetically encoded fluorescent probes or electrochemical methods[76,77]. HPLC offers high chemical sensitivity, but the temporal and especially spatial resolution is limited in addition to the invasiveness[76]. Genetically encoded fluorescence sensors have been very successful, but they so far do not emit in the NIR and cells or organisms have to be transfected. Electrochemical methods also suffer from limited spatial resolution and invasiveness[78]. Therefore, our NIR ratiometric approach adds a new technical possibility to the field.

Furthermore, the presented ratiometric approach offers several routes to further push the sensing performance. SWCNTs with quantum defects show higher quantum yields and increase brightness[38,65,79]. Furthermore, the selectivity is determined by the surface chemistry of SWCNTs. For DNA it is known that the sequence affects the selectivity for dopamine[29]. Further exploration of the sequence space as well as combination with quantum defects are likely to further increase figures of merit such as selectivity and robustness in complex environments such as cell medium. EB-NS are a new research topic and improvements in heterogeneity and colloidal stability/surface chemistry could enhance image quality by providing a more homogenous coating (FIGURE 4c)[52]. Functionalization of both nanomaterials to target the sensors to specific biological sites represents another opportunity[56].

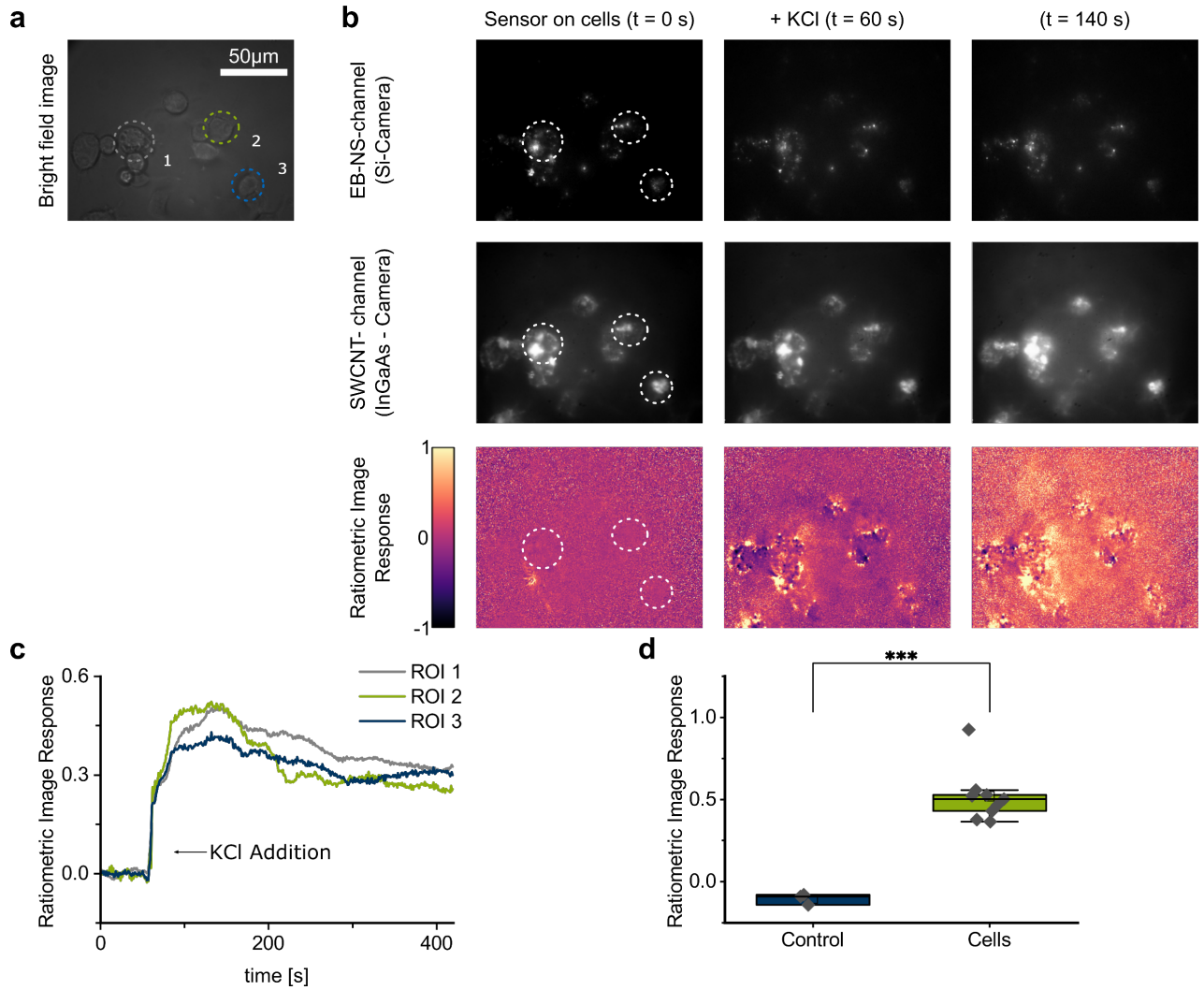

FIGURE 5: Ratiometric NIR imaging of dopamine release from neuronal cells. a) Brightfield image of differentiated Neuro 2a cells in HBSS with 2 mM CaCl2. Regions of interest are marked by dashed circles. b) Corresponding fluorescence images of EB-NS, SWCNTs and the resulting ratiometric response. c) Ratiometric image response from the marked regions of interest of cells over time shows release of dopamine after addition of 100 mM KCl. d) Ratiometric image response after KCl stimulation of Neuro 2a cells in contrast to a control (KCl addition to sensor without cells). Error = SD, n=3 for the control and n=9 for the cells.

For example, instead of relying on random physisorption on the cell surface one could target both EB-NS and SWCNTs to specific surface receptors or locations on cells. From a measurement perspective, fluorescence lifetime imaging (FLIM) could be an alternative and combined with the ratiometric approach. The differences in fluorescence lifetime varying by several orders of magnitude between SWCNTs and EB-NS is a major advantage here. SWCNT-based sensors have been used for FLIM by measuring the lifetimes on the order of 100 ps-1 ns, which can increase signal to noise ratios[41]. The much longer lifetime of EB-NS on the order of 10 µs could be differentiated and this combination holds the potential to further increase figures of merit such as temporal resolution[52].

Conclusion

In conclusion, we present a ratiometric NIR sensor enabling biosensing and imaging of the important neurotransmitter dopamine. The combination of single chirality (6,5)-SWCNTs as analyte sensitive nanomaterial and EB-NS as non-responding internal reference allows for robust and stable measurements. By using single chirality (6,5)-SWCNTs spectral overlap is avoided, which increases signal-to-noise ratios. The high photostability and fluorescence emission in the NIR of both nanomaterials further improves this approach providing measurements with high spatiotemporal resolution and minimal autofluorescence, scattering and light absorption. An advantage of the ratiometric system is that it compensates for fluctuations in environmental conditions and thus, provides improved imaging of the analyte (dopamine). In addition, we have shown that the ratiometric sensor can be applied to cellular systems to detect dopamine release. This ratiometric sensor paves the way for new insights into dopamine communication between neuronal cells and related diseases.

ASSOCIATED CONTENT

Additional spectral simulations, absorption spectra, additional fluorescence spectra, additional fluorescence microscopy images, details on fit parameters (PDF) and the original movies to fluorescence microscopy (AVI). This material is available free of charge via the Internet at http://pubs.acs.org.

AUTHOR INFORMATION

Corresponding Author

*sebastian.kruss@rub.de

Present Addresses

† Present Adress: Fraunhofer-Institute for Translational Medicine and Pharmacology, 37075 Göttingen, Germany
‡ Present Adress: Imec the Netherlands, 5656 AE Eindhoven, The Netherlands

Author Contributions

BH, JM and IS contributed equally.
SK conceived and coordinated the study with input from LE. BH exfoliated EB into EB-NS. PG and JG purified and functionalized SWCNTs. LS developed the ratiometric imaging setup. IS characterized the components and the sensor in dispersion with input from BH and PG. BH characterized the sensor on surface and under perturbations. JM and JG developed the sensor painting on cells. JM designed a protocol for differentiation of cells. JM and BH performed the cell experiments. BH, JM, IS and SK wrote the manuscript with input from all authors.

ACKNOWLEDGMENT

We thank Elena Polo for early experiments with EB-NS. Funded by the Deutsche Forschungsgemeinschaft (DFG, German Research Foundation) under Germany´s Excellence Strategy – EXC 2033 – 390677874 – RESOLV. This work is supported by the "Center for Solvation Science ZEMOS" funded by the German Federal Ministry of Education and Research BMBF and by the Ministry of Culture and Research of Nord Rhine-Westphalia. We are also grateful for the support of the VW foundation. We thank the DFG for funding within the Heisenberg program.

REFERENCES

(1) Smith, A. M.; Mancini, M. C.; Nie, S. Bioimaging: Second Window for in Vivo Imaging. Nat Nanotechnol 2009, 4 (11), 710–711. https://doi.org/10.1038/nnano.2009.326.

(2) Hong, G.; Antaris, A. L.; Dai, H. Near-Infrared Fluorophores for Biomedical Imaging. Nature Biomedical Engineering 2017 1:1 2017, 1 (1), 1–22. https://doi.org/10.1038/s41551-016-0010.

(3) O'Connell, M. J.; Bachilo, S. H.; Huffman, C. B.; Moore, V. C.; Strano, M. S.; Haroz, E. H.; Rialon, K. L.; Boul, P. J.; Noon, W. H.; Kittrell, C.; Ma, J.; Hauge, R. H.; Weisman, R. B.; Smalley, R. E. Band Gap Fluorescence from Individual Single-Walled Carbon Nanotubes. Science (1979) 2002, 297 (5581), 593–596. https://doi.org/10.1126/science.1072631.

(4) Ackermann, J.; Metternich, J. T.; Herbertz, S.; Kruss, S. Biosensing with Fluorescent Carbon Nanotubes. Angewandte Chemie - International Edition 2022, 61 (18), e202112372. https://doi.org/10.1002/anie.202112372.

(5) Baughman, R. H.; Zakhidov, A. A.; De Heer, W. A. Carbon Nanotubes - The Route toward Applications. Science (1979) 2002, 297 (5582), 787–792. https://doi.org/10.1126/science.1060928.

(6) Nißler, R.; Kurth, L.; Li, H.; Spreinat, A.; Kuhlemann, I.; Flavel, B. S.; Kruss, S. Sensing with Chirality-Pure Near-Infrared Fluorescent Carbon Nanotubes. Anal Chem 2021, 93 (16), 6446–6455. https://doi.org/10.1021/acs.analchem.1c00168.

(7) Amoroso, G.; Ye, Q.; Cervantes-Salguero, K.; Fernández, G.; Cecconello, A.; Palma, M. DNA-Powered Stimuli-Responsive Single-Walled Carbon Nanotube Junctions. Chemistry of Materials 2019, 31 (5), 1537–1542. https://doi.org/10.1021/ACS.CHEMMATER.8B04483.

(8) Antonucci, A.; Kupis-Rozmysłowicz, J.; Boghossian, A. A. Noncovalent Protein and Peptide Functionalization of Single-Walled Carbon Nanotubes for Biodelivery and Optical Sensing Applications. ACS Appl Mater Interfaces 2017, 9 (13), 11321–11331. https://doi.org/10.1021/ACSAMI.7B00810.

(9) Mann, F. A.; Horlebein, J.; Meyer, N. F.; Meyer, D.; Thomas, F.; Kruss, S. Carbon Nanotubes Encapsulated in Coiled-Coil Peptide Barrels. Chemistry – A European Journal 2018, 24 (47), 12241–12245. https://doi.org/10.1002/CHEM.201800993.

(10) Ford, W. E.; Jung, A.; Hirsch, A.; Graupner, R.; Scholz, F.; Yasuda, A.; Wessels, J. M. Urea-Melt Solubilization of Single-Walled Carbon Nanotubes. Advanced Materials 2006, 18 (9), 1193–1197. https://doi.org/10.1002/adma.200502257.

(11) Giacalone, F.; Campisciano, V.; Calabrese, C.; La Parola, V.; Syrgiannis, Z.; Prato, M.; Gruttadauria, M. Single-Walled Carbon Nanotube-Polyamidoamine Dendrimer Hybrids for Heterogeneous Catalysis. ACS Nano 2016, 10 (4), 4627–4636. https://doi.org/10.1021/ACSNANO.6B00936.

(12) Polo, E.; Kruss, S. Impact of Redox-Active Molecules on the Fluorescence of Polymer-Wrapped Carbon Nanotubes. Journal of Physical Chemistry C 2016, 120 (5), 3061–3070. https://doi.org/10.1021/ACS.JPCC.5B12183.

(13) Ackermann, J.; Metternich, J. T.; Herbertz, S.; Kruss, S. Biosensing with Fluorescent Carbon Nanotubes. Angew Chem Int Ed Engl 2022. https://doi.org/10.1002/anie.202112372.

(14) Wu, H.; Nißler, R.; Morris, V.; Herrmann, N.; Hu, P.; Jeon, S. J.; Kruss, S.; Giraldo, J. P. Monitoring Plant Health with Near-Infrared Fluorescent H2O2 Nanosensors. Nano Lett 2020, 20 (4), 2432–2442. https://doi.org/10.1021/acs.nanolett.9b05159.

(15) Lew, T. T. S.; Koman, V. B.; Silmore, K. S.; Seo, J. S.; Gordiichuk, P.; Kwak, S. Y.; Park, M.; Ang, M. C. Y.; Khong, D. T.; Lee, M. A.; Chan-Park, M. B.; Chua, N. H.; Strano, M. S. Real-Time Detection of Wound-Induced H2O2 Signalling Waves in Plants with Optical Nanosensors. Nat Plants

2020, 6 (4), 404–415. https://doi.org/10.1038/s41477-020-0632-4.

(16) Meier, J.; Stapleton, J.; Hofferber, E.; Haworth, A.; Kachman, S.; Iverson, N. M. Quantification of Nitric Oxide Concentration Using Single-Walled Carbon Nanotube Sensors. Nanomaterials 2021, 11 (1), 1–9. https://doi.org/10.3390/nano11010243.

(17) Giraldo, J. P.; Kruss, S. Nanosensors for Monitoring Plant Health. Nat Nanotechnol 2023, 18 (2), 107–108. https://doi.org/10.1038/s41565-022-01307-w.

(18) Safaee, M. M.; Gravely, M.; Roxbury, D. A Wearable Optical Microfibrous Biomaterial with Encapsulated Nanosensors Enables Wireless Monitoring of Oxidative Stress. Adv Funct Mater 2021, 31 (13), 2006254. https://doi.org/https://doi.org/10.1002/adfm.202006254.

(19) Heller, D. A.; Pratt, G. W.; Zhang, J.; Nair, N.; Hansborough, A. J.; Boghossian, A. A.; Reuel, N. F.; Barone, P. W.; Strano, M. S. Peptide Secondary Structure Modulates Single-Walled Carbon Nanotube Fluorescence as a Chaperone Sensor for Nitroaromatics. Proc Natl Acad Sci U S A 2011, 108 (21), 8544–8549. https://doi.org/10.1073/pnas.1005512108.

(20) Wong, M. H.; Giraldo, J. P.; Kwak, S. Y.; Koman, V. B.; Sinclair, R.; Lew, T. T. S.; Bisker, G.; Liu, P.; Strano, M. S. Nitroaromatic Detection and Infrared Communication from Wild-Type Plants Using Plant Nanobionics. Nature Materials 2016 16:2 2016, 16 (2), 264–272. https://doi.org/10.1038/nmat4771.

(21) Zhang, J.; Boghossian, A. A.; Barone, P. W.; Rwei, A.; Kim, J. H.; Lin, D.; Heller, D. A.; Hilmer, A. J.; Nair, N.; Reuel, N. F.; Strano, M. S. Single Molecule Detection of Nitric Oxide Enabled by d(AT)15 DNA Adsorbed to near Infrared Fluorescent Single-Walled Carbon Nanotubes. J Am Chem Soc 2011, 133 (3), 567–581. https://doi.org/10.1021/ja1084942.

(22) Amir, D.; Hendler-Neumark, A.; Wulf, V.; Ehrlich, R.; Bisker, G. Oncometabolite Fingerprinting Using Fluorescent Single-Walled Carbon Nanotubes. Adv Mater Interfaces 2022, 9 (4), 2101591. https://doi.org/https://doi.org/10.1002/admi.202101591.

(23) Zubkovs, V.; Schuergers, N.; Lambert, B.; Ahunbay, E.; Boghossian, A. A. Mediatorless, Reversible Optical Nanosensor Enabled through Enzymatic Pocket Doping. Small 2017, 13 (42), 1701654. https://doi.org/10.1002/SMLL.201701654.

(24) Ehrlich, R.; Hendler-Neumark, A.; Wulf, V.; Amir, D.; Bisker, G. Optical Nanosensors for Real-Time Feedback on Insulin Secretion by β-Cells. Small 2021, 17 (30), 2101660. https://doi.org/10.1002/smll.202101660.

(25) Bisker, G.; Dong, J.; Park, H. D.; Iverson, N. M.; Ahn, J.; Nelson, J. T.; Landry, M. P.; Kruss, S.; Strano, M. S. Protein-Targeted Corona Phase Molecular Recognition. Nat Commun 2016, 7, 1–14. https://doi.org/10.1038/ncomms10241.

(26) Gillen, A. J.; Boghossian, A. A. Non-Covalent Methods of Engineering Optical Sensors Based on Single-Walled Carbon Nanotubes . Frontiers in Chemistry 2019, 7.

(27) Pinals, R. L.; Yang, D.; Rosenberg, D. J.; Chaudhary, T.; Crothers, A. R.; Iavarone, A. T.; Hammel, M.; Landry, M. P. Quantitative Protein Corona Composition and Dynamics on Carbon Nanotubes in Biological Environments. Angewandte Chemie International Edition 2020, 59 (52), 23668–23677. https://doi.org/https://doi.org/10.1002/anie.202008175.

(28) Kruss, S.; Landry, M. P.; Vander Ende, E.; Lima, B. M. A.; Reuel, N. F.; Zhang, J.; Nelson, J.; Mu, B.; Hilmer, A.; Strano, M. Neurotransmitter Detection Using Corona Phase Molecular Recognition on Fluorescent Single-Walled Carbon Nanotube Sensors. J Am Chem Soc 2014, 136 (2), 713–724. https://doi.org/10.1021/ja410433b.

(29) Mann, F. A.; Herrmann, N.; Meyer, D.; Kruss, S. Tuning Selectivity of Fluorescent Carbon Nanotube-Based Neurotransmitter Sensors. Sensors 2017, Vol. 17, Page 1521 2017, 17 (7), 1521. https://doi.org/10.3390/S17071521.

(30) Dinarvand, M.; Neubert, E.; Meyer, D.; Selvaggio, G.; Mann, F. A.; Erpenbeck, L.; Kruss, S. Near-Infrared Imaging of Serotonin Release from Cells with Fluorescent Nanosensors. Nano Lett 2019, 19 (9), 6604–6611. https://doi.org/10.1021/acs.nanolett.9b02865.

(31) Jeong, S.; Yang, D.; Beyene, A. G.; Del Bonis-O'Donnell, J. T.; Gest, A. M. M.; Navarro, N.; Sun, X.; Landry, M. P. High-Throughput Evolution of near-Infrared Serotonin Nanosensors. Sci Adv 2019, 5 (12). https://doi.org/10.1126/sciadv.aay3771.

(32) Nißler, R.; Ackermann, J.; Ma, C.; Kruss, S. Prospects of Fluorescent Single-Chirality Carbon Nanotube-Based Biosensors. Anal Chem 2022, 94 (28), 9941–9951. https://doi.org/10.1021/ACS.ANALCHEM.2C01321.

(33) Nißler, R.; Bader, O.; Dohmen, M.; Walter, S. G.; Noll, C.; Selvaggio, G.; Groß, U.; Kruss, S. Remote near Infrared Identification of Pathogens with Multiplexed Nanosensors. Nat Commun 2020, 11 (1), 1–12. https://doi.org/10.1038/s41467-020-19718-5.

(34) Cho, S.-Y.; Gong, X.; Koman, V. B.; Kuehne, M.; Moon, S. J.; Son, M.; Lew, T. T. S.; Gordiichuk, P.; Jin, X.; Sikes, H. D.; Strano, M. S. Cellular Lensing and near Infrared Fluorescent Nanosensor Arrays to Enable Chemical Efflux Cytometry. Nat Commun 2021, 12 (1), 3079. https://doi.org/10.1038/s41467-021-23416-1.

(35) Metternich, J. T.; Hill, B.; Wartmann, J. A. C.; Ma, C.; Kruskop, R. M.; Neutsch, K.; Herbertz, S.; Kruss, S. Signal Amplification and Near-Infrared Translation of Enzymatic Reactions by Nanosensors. Angewandte Chemie - International Edition 2024, 63 (9). https://doi.org/10.1002/anie.202316965.

(36) Giraldo, J. P.; Landry, M. P.; Kwak, S. Y.; Jain, R. M.; Wong, M. H.; Iverson, N. M.; Ben-Naim, M.; Strano, M. S. A Ratiometric Sensor Using Single Chirality Near-Infrared Fluorescent Carbon Nanotubes: Application to in Vivo Monitoring. Small 2015, 11 (32), 3973–3984. https://doi.org/10.1002/smll.201403276.

(37) Settele, S.; Schrage, C. A.; Jung, S.; Michel, E.; Li, H.; Flavel, B. S.; Hashmi, A. S. K.; Kruss, S.; Zaumseil, J. Ratiometric Fluorescent Sensing of Pyrophosphate with Sp3-Functionalized Single-Walled Carbon Nanotubes. Nat Commun

2024, 15 (1), 1–13. https://doi.org/10.1038/s41467-024-45052-1.

(38) Spreinat, A.; Dohmen, M. M.; Lüttgens, J.; Herrmann, N.; Klepzig, L. F.; Nißler, R.; Weber, S.; Mann, F. A.; Lauth, J.; Kruss, S. Quantum Defects in Fluorescent Carbon Nanotubes for Sensing and Mechanistic Studies. Journal of Physical Chemistry C 2021, 125 (33), 18341–18351. https://doi.org/10.1021/acs.jpcc.1c05432.

(39) Nißler, R.; Müller, A. T.; Dohrman, F.; Kurth, L.; Li, H.; Cosio, E. G.; Flavel, B. S.; Giraldo, J. P.; Mithöfer, A.; Kruss, S. Detection and Imaging of the Plant Pathogen Response by Near-Infrared Fluorescent Polyphenol Sensors. Angewandte Chemie - International Edition 2022, 61 (2), e202108373. https://doi.org/10.1002/anie.202108373.

(40) Ma, C.; Mohr, J. M.; Lauer, G.; Metternich, J. T.; Neutsch, K.; Ziebarth, T.; Reiner, A.; Kruss, S. Ratiometric Imaging of Catecholamine Neurotransmitters with Nanosensors. Nano Lett 2024, 24 (7), 2400–2407. https://doi.org/10.1021/acs.nanolett.3c05082.

(41) Sistemich, L.; Galonska, P.; Stegemann, J.; Ackermann, J.; Kruss, S. Near-Infrared Fluorescence Lifetime Imaging of Biomolecules with Carbon Nanotubes. Angewandte Chemie - International Edition 2023, 62 (24), e202300682. https://doi.org/10.1002/anie.202300682.

(42) Shao, W.; Shurin, M. R.; Wheeler, S. E.; He, X.; Star, A. Rapid Detection of SARS-CoV-2 Antigens Using High-Purity Semiconducting Single-Walled Carbon Nanotube-Based Field-Effect Transistors. ACS Appl Mater Interfaces 2021, 13 (8), 10321–10327. https://doi.org/10.1021/acsami.0c22589.

(43) Galassi, T. V.; Antman-Passig, M.; Yaari, Z.; Jessurun, J.; Schwartz, R. E.; Heller, D. A. Long-Term in Vivo Biocompatibility of Single-Walled Carbon Nanotubes. PLoS One 2020, 15 (5), e0226791. https://doi.org/10.1371/journal.pone.0226791.

(44) Johnson-McDaniel, D.; Barrett, C. A.; Sharafi, A.; Salguero, T. T. Nanoscience of an Ancient Pigment. J Am Chem Soc 2013, 135 (5), 1677–1679. https://doi.org/10.1021/ja310587c.

(45) Selvaggio, G.; Kruss, S. Preparation, Properties and Applications of near-Infrared Fluorescent Silicate Nanosheets. Nanoscale 2022, 14 (27), 9553–9575. https://doi.org/10.1039/d2nr02967g.

(46) Berke, H. The Invention of Blue and Purple Pigments in Ancient Times. Chem Soc Rev 2007, 36, 15–30. https://doi.org/10.1039/b606268g.

(47) Nicola, M.; Gobetto, R.; Masic, A. Egyptian Blue, Chinese Blue, and Related Two-Dimensional Silicates: From Antiquity to Future Technologies. Part A: General Properties and Historical Uses. Rend Lincei Sci Fis Nat 2023. https://doi.org/10.1007/s12210-023-01153-5.

(48) Kendrick, E.; Kirk, C. J.; Dann, S. E. Structure and Colour Properties in the Egyptian Blue Family, M1-XM′xCuSi4O10, as a Function of M, M′ Where M, M′ = Ca, Sr and Ba. Dyes and Pigments 2007, 73 (1), 13–18. https://doi.org/10.1016/j.dyepig.2005.10.006.

(49) Pozza, G.; Ajò, D.; Chiari, G.; De Zuane, F.; Favaro, M. Photoluminescence of the Inorganic Pigments Egyptian Blue, Han Blue and Han Purple. J Cult Herit 2000, 1 (4), 393–398. https://doi.org/10.1016/S1296-2074(00)01095-5.

(50) Borisov, S. M.; Würth, C.; Resch-Genger, U.; Klimant, I. New Life of Ancient Pigments: Application in High-Performance Optical Sensing Materials. Anal Chem 2013, 85 (19), 9371–9377. https://doi.org/10.1021/ac402275g.

(51) Accorsi, G.; Verri, G.; Bolognesi, M.; Armaroli, N.; Clementi, C.; Miliani, C.; Romani, A. The Exceptional Near-Infrared Luminescence Properties of Cuprorivaite (Egyptian Blue). Chemical Communications 2009, No. 23, 3392–3394. https://doi.org/10.1039/b902563d.

(52) Selvaggio, G.; Weitzel, M.; Oleksiievets, N.; Oswald, T. A.; Nißler, R.; Mey, I.; Karius, V.; Enderlein, J.; Tsukanov, R.; Kruss, S. Photophysical Properties and Fluorescence Lifetime Imaging of Exfoliated Near-Infrared Fluorescent Silicate Nanosheets. Nanoscale Adv 2021, 3 (15), 4541–4553. https://doi.org/10.1039/d1na00238d.

(53) Nicola, M.; Garino, C.; Mittman, S.; Priola, E.; Palin, L.; Ghirardello, M.; Damagatla, V.; Nevin, A.; Masic, A.; Comelli, D.; Gobetto, R. Increased NIR Photoluminescence of Egyptian Blue via Matrix Effect Optimization. Mater Chem Phys 2024, 313, 128710. https://doi.org/https://doi.org/10.1016/j.matchemphys.2023.128710.

(54) Hill, B.; Abraham, S.; Akhtar, A.; Selvaggio, G.; Tschulik, K.; Kruss, S. Surfactant Assisted Exfoliation of near Infrared Fluorescent Silicate Nanosheets. RSC Adv 2023, 13 (30), 20916–20925. https://doi.org/10.1039/d3ra04083f.

(55) Selvaggio, G.; Chizhik, A.; Nißler, R.; Kuhlemann, L.; Meyer, D.; Vuong, L.; Preiß, H.; Herrmann, N.; Mann, F. A.; Lv, Z.; Oswald, T. A.; Spreinat, A.; Erpenbeck, L.; Großhans, J.; Karius, V.; Janshoff, A.; Pablo Giraldo, J.; Kruss, S. Exfoliated near Infrared Fluorescent Silicate Nanosheets for (Bio)Photonics. Nat Commun 2020, 11 (1), 1495. https://doi.org/10.1038/s41467-020-15299-5.

(56) Selvaggio, G.; Herrmann, N.; Hill, B.; Dervişoğlu, R.; Jung, S.; Weitzel, M.; Dinarvand, M.; Stalke, D.; Andreas, L.; Kruss, S. Covalently Functionalized Egyptian Blue Nanosheets for Near-Infrared Bioimaging. ACS Appl Bio Mater 2023, 6 (1), 309–317. https://doi.org/10.1021/acsabm.2c00872.

(57) Bigdeli, A.; Ghasemi, F.; Abbasi-Moayed, S.; Shahrajabian, M.; Fahimi-Kashani, N.; Jafarinejad, S.; Farahmand Nejad, M. A.; Hormozi-Nezhad, M. R. Ratiometric Fluorescent Nanoprobes for Visual Detection: Design Principles and Recent Advances - A Review. Anal Chim Acta 2019, 1079, 30–58. https://doi.org/10.1016/j.aca.2019.06.035.

(58) Lee, M. H.; Kim, J. S.; Sessler, J. L. Small Molecule-Based Ratiometric Fluorescence Probes for Cations, Anions, and Biomolecules. Chem Soc Rev 2015, 44 (13), 4185–4191. https://doi.org/10.1039/c4cs00280f.

(59) Huang, X.; Song, J.; Yung, B. C.; Huang, X.; Xiong, Y.; Chen, X. Ratiometric Optical Nanoprobes Enable Accurate Molecular Detection and Imaging. Chem Soc Rev 2018, 47 (8), 2873–2920. https://doi.org/10.1039/C7CS00612H.

(60) Jin, H.; Jiang, X.; Sun, Z.; Gui, R. Phosphorescence-Based Ratiometric Probes: Design, Preparation and Applications in Sensing, Imaging and Biomedicine Therapy. Coord Chem Rev 2021, 431. https://doi.org/10.1016/j.ccr.2020.213694.

(61) Peng, R.; Si, Y.; Deng, T.; Zheng, J.; Li, J.; Yang, R.; Tan, W. A Novel SERS Nanoprobe for the Ratiometric Imaging of Hydrogen Peroxide in Living Cells. Chemical Communications 2016, 52 (55), 8553–8556. https://doi.org/10.1039/C6CC03412H.

(62) Zhu, X.; Han, L.; Liu, H.; Sun, B. A Smartphone-Based Ratiometric Fluorescent Sensing System for on-Site Detection of Pyrethroids by Using Blue-Green Dual-Emission Carbon Dots. Food Chem 2022, 379, 132154. https://doi.org/10.1016/j.foodchem.2022.132154.

(63) Antaris, A. L.; Robinson, J. T.; Yaghi, O. K.; Hong, G.; Diao, S.; Luong, R.; Dai, H. Ultra-Low Doses of Chirality Sorted (6,5) Carbon Nanotubes for Simultaneous Tumor Imaging and Photothermal Therapy. ACS Nano 2013, 7 (4), 3644–3652. https://doi.org/10.1021/nn4006472.

(64) Li, H.; Gordeev, G.; Garrity, O.; Reich, S.; Flavel, B. S. Separation of Small-Diameter Single-Walled Carbon Nanotubes in One to Three Steps with Aqueous Two-Phase Extraction. ACS Nano 2019, 13 (2), 2567–2578. https://doi.org/10.1021/acsnano.8b09579.

(65) Ma, C.; Schrage, C. A.; Gretz, J.; Akhtar, A.; Sistemich, L.; Schnitzler, L.; Li, H.; Tschulik, K.; Flavel, B. S.; Kruss, S. Stochastic Formation of Quantum Defects in Carbon Nanotubes. ACS Nano 2023, 17 (16), 15989–15998. https://doi.org/10.1021/acsnano.3c04314.

(66) Nißler, R.; Mann, F. A.; Chaturvedi, P.; Horlebein, J.; Meyer, D.; Vuković, L.; Kruss, S. Quantification of the Number of Adsorbed DNA Molecules on Single-Walled Carbon Nanotubes. The Journal of Physical Chemistry C 2019, 123 (8), 4837–4847. https://doi.org/10.1021/acs.jpcc.8b11058.

(67) Elizarova, S.; Chouaib, A. A.; Shaib, A.; Hill, B.; Mann, F.; Brose, N.; Kruss, S.; Daniel, J. A. A Fluorescent Nanosensor Paint Detects Dopamine Release at Axonal Varicosities with High Spatiotemporal Resolution. Proc Natl Acad Sci U S A 2022, 119 (22), e2202842119. https://doi.org/10.1073/pnas.2202842119.

(68) Kruss, S.; Salem, D. P.; Vuković, L.; Lima, B.; Ende, E. Vander; Boyden, E. S.; Strano, M. S. High-Resolution Imaging of Cellular Dopamine Efflux Using a Fluorescent Nanosensor Array. Proceedings of the National Academy of Sciences 2017, 114 (8), 1789–1794. https://doi.org/10.1073/pnas.1613541114.

(69) Tremblay, R. G.; Sikorska, M.; Sandhu, J. K.; Lanthier, P.; Ribecco-Lutkiewicz, M.; Bani-Yaghoub, M. Differentiation of Mouse Neuro 2A Cells into Dopamine Neurons. J Neurosci Methods 2010, 186 (1), 60–67. https://doi.org/10.1016/j.jneumeth.2009.11.004.

(70) Curtin, B. F.; Pal, N.; Gordon, R. K.; Nambiar, M. P. Forskolin, an Inducer of CAMP, up-Regulates Acetylcholinesterase Expression and Protects against Organophosphate Exposure in Neuro 2A Cells. Mol Cell Biochem 2006, 290 (1–2), 23–32. https://doi.org/10.1007/s11010-005-9084-4.

(71) Pang, Z. P.; Südhof, T. C. Cell Biology of Ca2+-Triggered Exocytosis. Curr Opin Cell Biol 2010, 22 (4), 496–505. https://doi.org/https://doi.org/10.1016/j.ceb.2010.05.001.

(72) Costantini, L. M.; Snapp, E. L. Fluorescent Proteins in Cellular Organelles: Serious Pitfalls and Some Solutions. DNA Cell Biol 2013, 32 (11), 622–627. https://doi.org/10.1089/dna.2013.2172.

(73) Godin, A. G.; Varela, J. A.; Gao, Z.; Danné, N.; Dupuis, J. P.; Lounis, B.; Groc, L.; Cognet, L. Single-Nanotube Tracking Reveals the Nanoscale Organization of the Extracellular Space in the Live Brain. Nat Nanotechnol 2017, 12 (3), 238–243. https://doi.org/10.1038/nnano.2016.248.

(74) Paviolo, C.; Cognet, L. Near-Infrared Nanoscopy with Carbon-Based Nanoparticles for the Exploration of the Brain Extracellular Space. Neurobiol Dis 2021, 153, 105328. https://doi.org/https://doi.org/10.1016/j.nbd.2021.105328.

(75) Rana, S.; Elci, S. G.; Mout, R.; Singla, A. K.; Yazdani, M.; Bender, M.; Bajaj, A.; Saha, K.; Bunz, U. H. F.; Jirik, F. R.; Rotello, V. M. Ratiometric Array of Conjugated Polymers-Fluorescent Protein Provides a Robust Mammalian Cell Sensor. J Am Chem Soc 2016, 138 (13), 4522–4529. https://doi.org/10.1021/JACS.6B00067.

(76) He, Q.; Li, M.; Wang, X.; Xia, Z.; Du, Y.; Li, Y.; Wei, L.; Shang, J. A Simple, Efficient and Rapid HPLC–UV Method for the Detection of 5-HT in RIN-14B Cell Extract and Cell Culture Medium. BMC Chem 2019, 13 (1), 76. https://doi.org/10.1186/s13065-019-0591-x.

(77) Stapleton, J. A.; Hofferber, E. M.; Meier, J.; Ramirez, I. A.; Iverson, N. M. Single-Walled Carbon Nanotube Sensor Platform for the Study of Extracellular Analytes. ACS Appl Nano Mater 2021, 4 (1), 33–42. https://doi.org/10.1021/acsanm.0c01998.

(78) Cheng, L.; Jin, R.; Jiang, D.; Zhuang, J.; Liao, X.; Zheng, Q. Scanning Electrochemical Cell Microscopy Platform with Local Electrochemical Impedance Spectroscopy. Anal Chem 2021, 93 (49), 16401–16408. https://doi.org/10.1021/acs.analchem.1c02972.

(79) Piao, Y.; Meany, B.; Powell, L. R.; Valley, N.; Kwon, H.; Schatz, G. C.; Wang, Y. Brightening of Carbon Nanotube Photoluminescence through the Incorporation of Sp3 Defects. Nat Chem 2013, 5 (10), 840–845. https://doi.org/10.1038/nchem.1711.

Table of Contents artwork